Supplementary Table Captions

Supplementary Table 1: Numerical data underlying Figure 1a-b. For each (tissue-gene fine-mapping method, eQTL sample size, PIP threshold) triplet, we report the average empirical False Discovery Rate (FDR) across 100 default simulations, as well as the 95% confidence interval lower and upper bounds on the average empirical FDR. We consider the tissue-gene fine-mapping methods TGFM (Gene-Tissue), FOCUS-TG, FOCUS, and coloc.

Supplementary Table 2: Numerical data underlying Figure 1c-d. For each (tissue-gene fine-mapping method, eQTL sample size, PIP threshold) triplet, we report the average power for detecting causal gene-tissue pairs across 100 default simulations, as well as the 95% confidence interval lower and upper bounds on the average power. We consider the tissue-gene fine-mapping methods TGFM (Gene-Tissue), FOCUS-TG, FOCUS, and coloc.

Supplementary Table 3: Numerical data underlying Figure 2a-b. For each (genetic element, eQTL sample size, PIP threshold) triplet, we report the average empirical False Discovery Rate (FDR) across 100 default simulations, as well as the 95% confidence interval lower and upper bounds on the average empirical FDR. Genetic elements include gene-tissue pairs, genes, and non-mediated genetic variants.

Supplementary Table 4: Numerical data underlying Figure 2c-d. For each (genetic element, eQTL sample size, PIP threshold) triplet, we report the average power across 100 default simulations, as well as the 95% confidence interval lower and upper bounds on the average power. Genetic elements include gene-tissue pairs, genes, and non-mediated genetic variants.

Supplementary Table 5: Description of 45 analyzed UK Biobank diseases and traits. For each of the 45 analyzed UK Biobank diseases and complex traits, we report the study name, the study sample size, and study's estimated heritability.

Supplementary Table 6: Description of GTEx tissues. For each of the 38 GTEx metatissues we report the metatissue sample size, the composite tissues defining the metatissue (','-seperated if multiple composite tissues), the sample size of each composite tissue (','-seperated if multiple composite tissues), and the number of genes with a gene model in the metatissue.

Supplementary Table 7: TGFM runtimes for UKBB traits. We split TGFM into 3 tasks. For each of the three tasks, we report the total TGFM runtime in hours. The first task is running TGFM step 1 and TGFM step 2 (in TGFM step 1, we apply SuSiE to perform eQTL fine-mapping of each gene-tissue pair in the external gene expression data set (estimating a posterior distribution of the causal cis-eQTL effect sizes for each gene-tissue pair). In TGFM step 2, we randomly sample 100 cis-predicted expression models for each gene-tissue pair from the posterior distributions of causal cis-eQTL effect sizes estimated in TGFM step 1). We report the runtime of the first task for a

single, average sample size GTEx tissue: Heart Left Ventricle. We note that this task can be parallelized across genes (i.e., each gene can be run independently). The second task is running the TGFM tissue specific prior. We report the runtime of the second task for a single, average heritability trait: Total cholesterol. We note that this task can be parallelized across fine-mapping windows (i.e., each fine-mapping window can be run independently). The third task is running TGFM step 3 and TGFM step 4 (In TGFM step 3, we apply SuSiE to perform disease fine-mapping in the target data set (estimating the PIP of each genetic element) 100 times, iterating over the sampled cis-predicted expression models for each gene-tissue pair from TGFM step 2. In TGFM step 4, we average the results of TGFM step 3 across the 100 disease fine-mapping runs.). We report the runtime of the third task for a single, average heritability trait: Total cholesterol. We note that this task can be parallelized across fine-mapping windows (i.e., each fine-mapping window can be run independently). Runtimes do not include computing LD matrices, as that is considered part of the input to TGFM (see data availability).

Supplementary Table 8: Number of fine-mapped genetic elements for UK Biobank diseases and traits. For each trait-genetic element pair with TGFM PIP ≥ 0.2 corresponding to one of the 16 independent traits (Figure 3), we report the corresponding genetic element class (ie. gene-tissue, gene, or variant), the trait, and the TGFM PIP.

Supplementary Table 9: Proportion of fine-mapped gene-tissue pairs in each tissue for UK Biobank diseases and traits. For each trait-tissue pair, we report the proportion of the trait's fine-mapped gene-tissue pairs in the tissue (proportions for each trait were calculated by counting the number of gene-tissue pairs with TGFM PIP > 0.5 in each tissue and normalizing the counts across tissues), the p-value of the trait-tissue pair determined by applying genomic bootstrapping to the TGFM tissue-specific prior, and the FDR significance (calculated by applying Benjamini-Hochberg correction for 38 tissues; '**' represents FDR ≤ 0.05, '**' represents FDR ≤ 0.2, 'null' denotes FDR $>$ 0.2).

Supplementary Table 10: Average correlation in cis-predicted gene expression between pairs of GTEx tissues. For each pair of tissues, we report the average correlation in cis-predicted gene expression across genes (we only consider genes with a cis-predicted expression model in both tissues) and the number of genes the average is taken across. We observed that several of the low sample size tissues (e.g. uterus, vagina, artery coronary, minor salivary gland, prostate; Supplementary Table 6) have high correlation with nearly all other tissues. We assume this is a technical artifact of low sample size tissues being limited to discovering very large eQTL effect size variants (due to statistical power), which are known to be less tissue-specific than small eQTL effect size variants.

Supplementary Table 11: Average PoPS score of genes stratified by TGFM (Gene) PIP. For each TGFM (Gene) PIP bin (we use the following bins: $0 \leq PIP < 0.01$, $0.01 \leq PIP < 0.25$, $0.25 \leq PIP < 0.5$, $0.5 \leq PIP < 0.7$, $0.7 \leq PIP < 0.9$, and $0.9 \leq PIP$), we

report the average PoPS score of all gene-trait pairs in the bin across 16 independent traits, and the standard error of the average PoPS score.

Supplementary Table 12: Enrichment of fine-mapped TGFM genes within non-disease-specific gene sets. For each (non-disease-specific gene set, TGFM PIP threshold) pair, we report enrichment statistics corresponding to enrichment of genes with TGFM (Gene) PIP > TGFM PIP threshold within the non-disease-specific gene set meta-analyzed over 16 independent traits. Enrichment statistics consist of enrichment odds ratio, enrichment odds ratio 95% confidence interval lower bound, enrichment odds ratio 95% confidence interval upper bound, and enrichment p-value. Odds ratios and standard errors on the odds ratio were computed using logistic regression.

Supplementary Table 13: Numerical data underlying examples of fine-mapped gene-tissue-disease triplets identified by TGFM. For each genetic element-disease pair visualized in Figure 5, we report the -log10(p-value) of the marginal association between the genetic element and disease (we report the median -log10(TWAS p-value) across the 100 sets of sampled cis-predicted expression for gene-tissue pairs and the -log10(GWAS p-value) for variants), the location of the genetic element (we report the gene's TSS for gene-tissue pairs and the variant location for variants), and the TGFM PIP of the genetic element.

Supplementary Table 14: Description of PBMC cell types from Perez et al. Science 2022. For each of the 9 PBMC cell types we report the sample size, the average number of cells per donor, and the number of genes with a gene model.

Supplementary Table 15: Number of fine-mapped gene-PBMC cell type pairs for all 45 UK Biobank diseases and traits. For each gene-PBMC cell type-trait triplets with TGFM PIP $\geq$ 0.2 corresponding to one of the 45 analyzed UKBB diseases and complex traits, we report the corresponding trait, PBMC cell type, and the TGFM PIP.

Supplementary Table 16: Numerical data underlying examples of fine-mapped gene-PBMC cell type-disease triplets identified by TGFM. For each genetic element-disease pair visualized in Figure 7, we report the -log10(p-value) of the marginal association between the genetic element and disease (we report the median -log10(TWAS p-value) across the 100 sets of sampled cis-predicted expression for gene-tissue pairs and gene-PBMC cell type pairs and the -log10(GWAS p-value) for variants), the location of the genetic element (we report the gene's TSS for gene-tissue pairs and gene-PBMC cell type pairs, and the variant location for variants), and the TGFM PIP of the genetic element.

Supplementary Table 17: Significance of tissue-specific prior for each trait-tissue pair and each trait-PBMC cell type pair. For each trait-tissue pair and each trait-PBMC cell type pair, we report the p-value of the trait-tissue pair or the trait-PBMC cell type pair determined by applying genomic bootstrapping to the TGFM tissue-specific prior, and the Bonferroni corrected p-value (calculated by correcting for 38 tissues and 9 cell types).

Supplementary Note

Additional examples of fine-mapped gene-tissue pairs

We highlight 6 additional examples of fine-mapped (PIP > 0.5) gene-tissue-trait triplets that recapitulate known biology or nominate biologically plausible mechanisms. First, TGFM fine-mapped *SMIM1* in whole blood for Red blood cell count (Supplementary Figure 18a; gene-tissue PIP: 0.78; gene PIP: 0.84). *SMIM1* was previously reported to encode the Vel blood group protein involved in red blood cell formation[1,2], and has previously been linked to Red blood cell count in genetic association studies[3,4]. Whole blood was also identified as a Red blood cell count-critical tissue genome-wide (proportion of fine-mapped gene-tissue pairs = 0.23, bootstrap p = 0.01 for tissue-specific prior; Supplementary Figure 14), an intuitive finding given that red blood cells constitute a large proportion of whole blood tissue. There exist 25 other gene-tissue within 1 Mb of the TSS of *SMIM1* (2 of which correspond to *SMIM1* in a tissue other than whole blood) that had significant TWAS p-values ($p \leq 0.05 / 119{,}270 = 4.2 \times 10^{-7}$) but were not fine-mapped by TGFM (all with PIP ≤ 0.01), underscoring the benefit of joint fine-mapping of gene-tissue pairs. TGFM also fine-mapped one non-mediated variant (rs1569419; PIP: 1.0) within 1 Mb of the TSS of *SMIM1*, perhaps due to finite eQTL sample size and/or absence of the causal cell-type or context in GTEx expression data (see Discussion).

Second, TGFM fine-mapped *NYNRIN* in liver for Total cholesterol (Supplementary Figure 18b; gene-tissue PIP: 0.70; gene PIP: 0.98). *NYNRIN* has previously been linked to LDL cholesterol in genetic association studies[5,6]. Liver was also identified as a Total

cholesterol-critical tissue genome-wide (proportion of fine-mapped gene-tissue pairs = 0.60, bootstrap p = 2.0×10^{-6} for tissue-specific prior; Supplementary Figure 14). There exist 2 other gene-tissue within 1 Mb of the TSS of *NYNRIN* that had significant TWAS p-values ($p \leq 0.05 / 119{,}270 = 4.2 \times 10^{-7}$) but were not fine-mapped by TGFM (both with PIP ≤ 0.01), underscoring the benefit of joint fine-mapping of gene-tissue pairs.

Third, TGFM fine-mapped *ACE* in adrenal gland for Hypertension (Supplementary Figure 18c; gene-tissue PIP: 0.61; gene PIP: 0.82). The involvement of *ACE* in hypertension via regulation of Aldosterone production in the adrenal gland is well-studied, and *ACE* inhibitors are a popular drug used to treat hypertension[7–9]. *ACE* has previously been linked to Hypertension in genetic association studies[10]. Adrenal gland was also identified as a Hypertension-critical tissue genome-wide (proportion of fine-mapped gene-tissue pairs = 0.43, bootstrap p = 0.03 for tissue-specific prior; Supplementary Figure 14).

Fourth, TGFM fine-mapped *LIPC* in liver for Vitamin D level (Supplementary Figure 18d; gene-tissue PIP: 0.83; gene PIP: 0.87). The involvement of *LIPC* in lipid metabolism is well-studied[11,12], and other work has demonstrated the impact of lipid biology on Vitamin D levels; Vitamin D is a fat-soluble hormone[13,14]. *LIPC* has previously been linked to Vitamin D level in genetic association studies[13,15]. Liver was also identified as a Vitamin D level-critical tissue genome-wide (proportion of fine-mapped gene-tissue pairs = 0.14, bootstrap p = 0.02 for tissue-specific prior; Supplementary Figure 14). We note that we have highlighted two fine-mapped gene-tissue pairs for Vitamin D level (Figure 5c and

Supplementary Figure 18d) involving two different tissues (skin (sun exposed) and liver); this demonstrates the advantages of TGFM over a two-step approach of separately identifying the causal gene using a gene-level fine-mapping[16] and identifying the causal tissue using a method for identifying trait-critical tissues[17–19].

Fifth, TGFM fine-mapped *NRP2* in lung for FEV1:FVC (ratio of forced expiratory volume in 1 second to forced vital capacity; Supplementary Figure 18e; gene-tissue PIP: 0.98; gene PIP: 0.99). Recent work has demonstrated the role of *NRP2* in regulating airway inflammatory responses in the lungs[20,21], but *NRP2* has not previously been linked to FEV1:FVC to our knowledge. Lung was also identified as a FEV1:FVC-critical tissue genome-wide (proportion of fine-mapped gene-tissue pairs = 0.13, bootstrap p = 0.002 for tissue-specific prior; Supplementary Figure 14).

Sixth, TGFM fine-mapped *SIX3* in pancreas for HbA1c levels (Supplementary Figure 18f; gene-tissue PIP: 0.67; gene PIP: 0.67). Previous work has demonstrated that *SIX3* regulates the functional maturity of human pancreatic β cells[22,23], but *SIX3* has not previously been linked to *HbA1c* levels in genetic association studies to our knowledge. Pancreas was suggestively implicated as a HbA1c-critical tissue genome-wide (proportion of fine-mapped gene-tissue pairs = 0.13, bootstrap p = 0.06 for tissue-specific prior; Supplementary Figure 14).

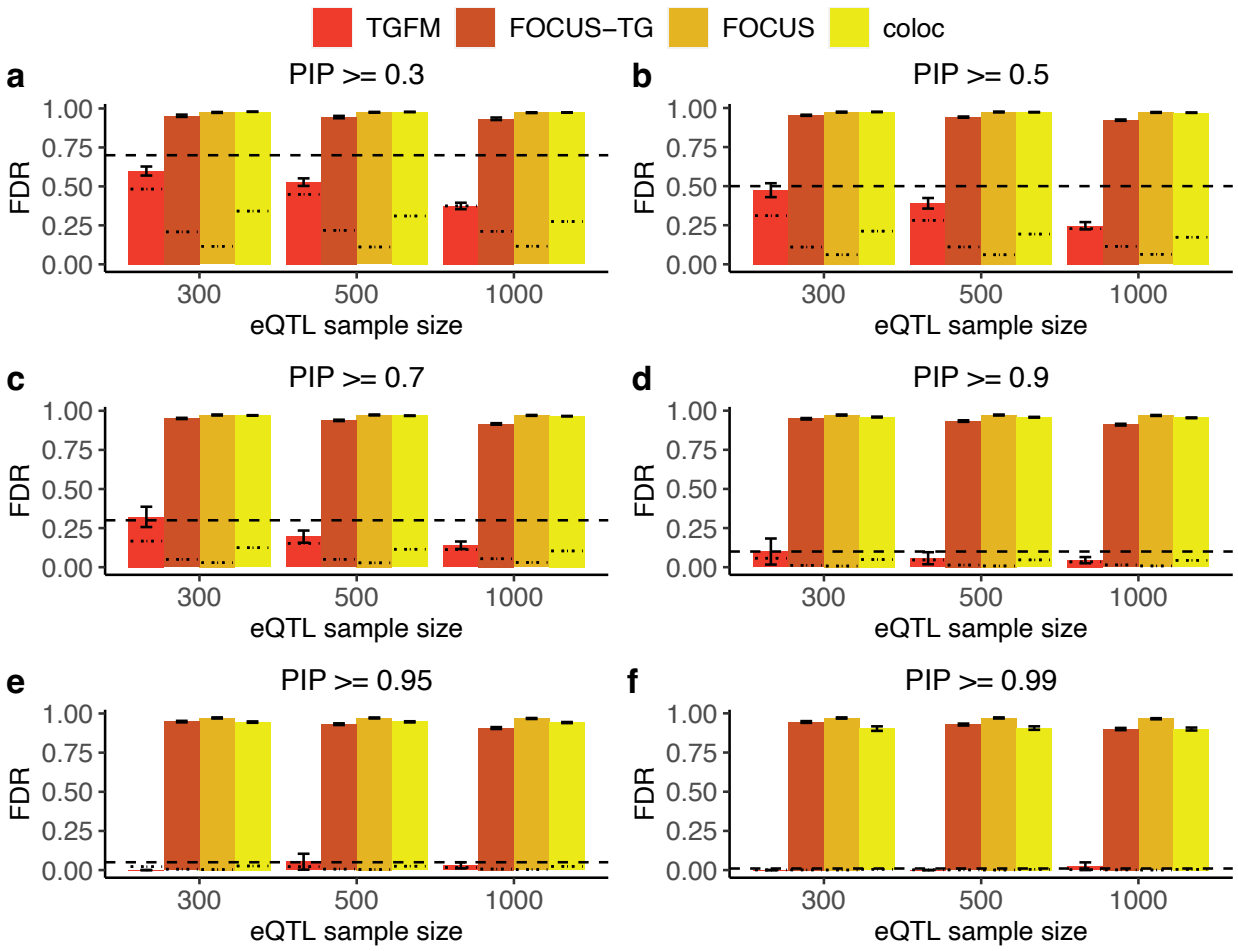

Supplementary Figure 1: Calibration of tissue-gene fine-mapping methods at various PIP thresholds in simulations. Average gene-tissue pair fine-mapping FDR across 100 simulations for various fine-mapping methods (see legend) across eQTL sample sizes (x-axis) at PIP=0.3 **(a)**, PIP=0.5 **(b)**, PIP=0.7 **(c)**, PIP=0.9 **(d)**, PIP=0.95 **(e)**, and PIP=0.99 **(f)**. In each plot, the single thick-dashed horizontal line (1 – PIP) threshold (see main text). The thin dashed lines specific to each bar denotes (1 – average PIP) (where average is taken across all genetic elements belonging to that bar; see main text). Error bars denote 95% confidence intervals. This supplementary figure is the same as Fig. 1a-b, except it includes more PIP thresholds, as well as dashed lines denoting (1 – average PIP).

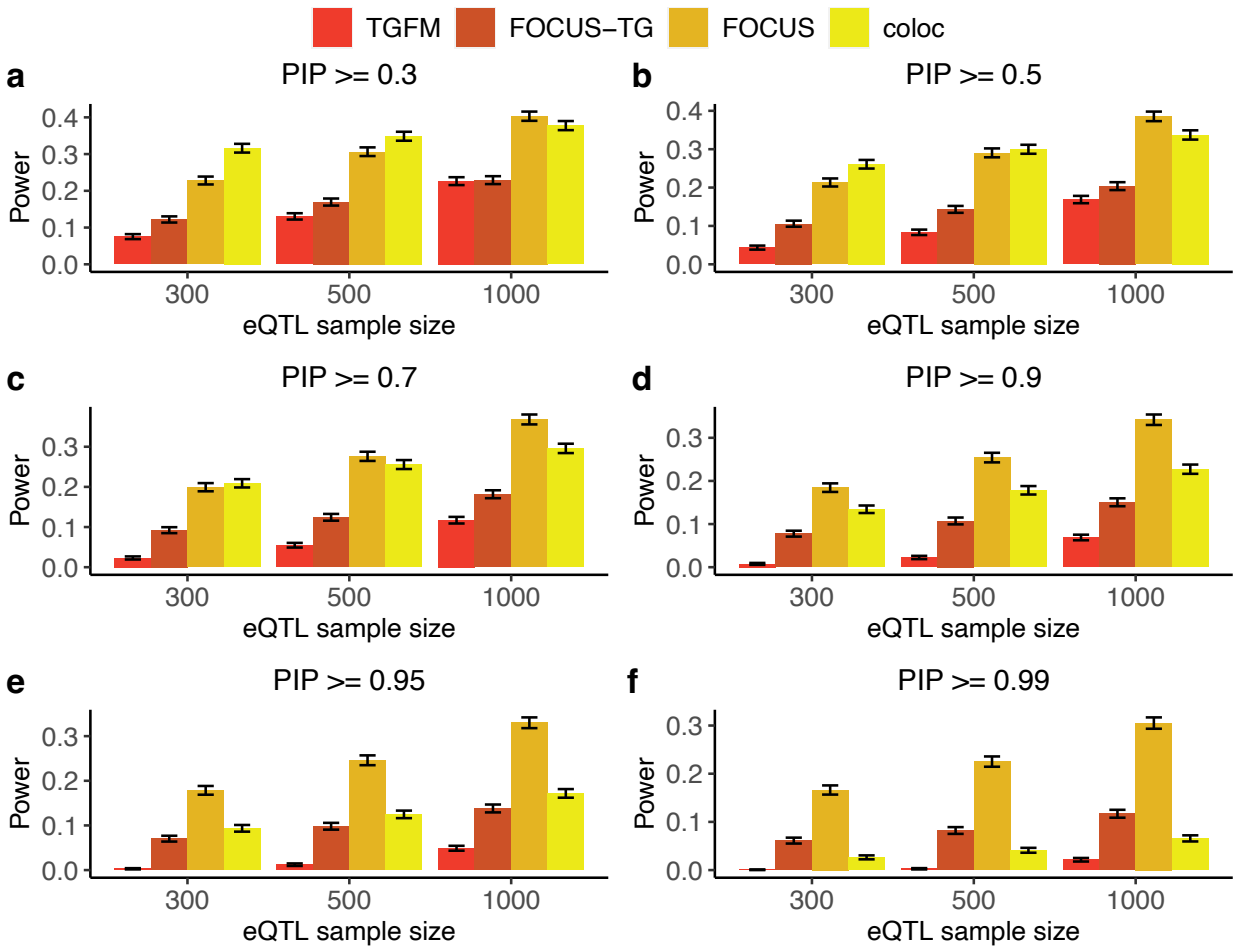

Supplementary Figure 2: Power of tissue-gene fine-mapping methods at various PIP thresholds in simulations. Average gene-tissue pair fine-mapping power across 100 simulations for various fine-mapping methods (see legend) across eQTL sample sizes (x-axis) at PIP=0.3 **(a)**, PIP=0.5 **(b)**, PIP=0.7 **(c)**, PIP=0.9 **(d)**, PIP=0.95 **(e)**, and PIP=0.99 **(f)**. Error bars denote 95% confidence intervals. This supplementary figure is the same as Fig. 1c-d, except it includes more PIP thresholds.

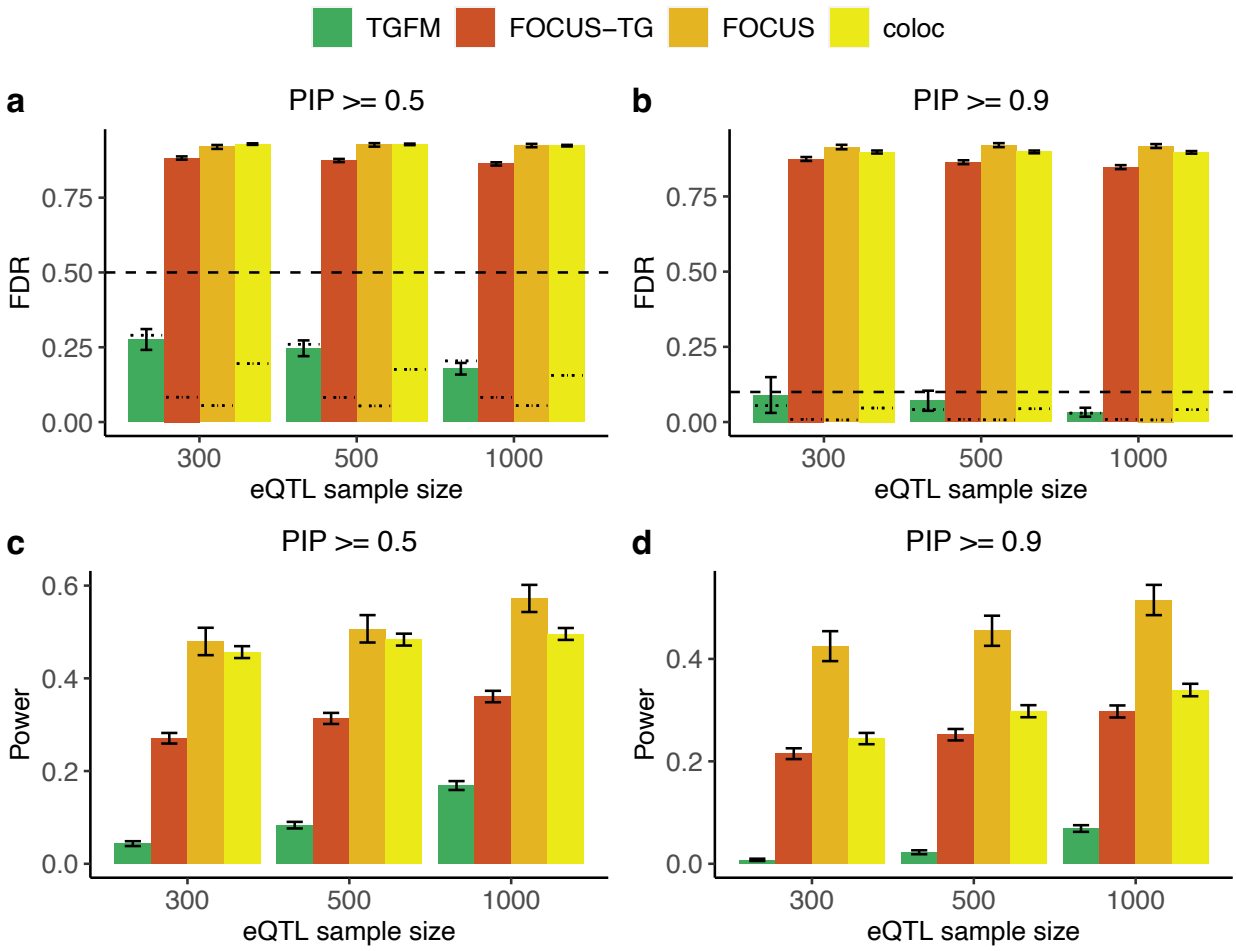

Supplementary Figure 3: Calibration and power of gene fine-mapping methods at various PIP thresholds in simulations. (a,b) Average *gene* fine-mapping FDR across 100 simulations for various fine-mapping methods (see legend) across eQTL sample sizes (x-axis) at PIP=0.5 **(a)** and PIP=0.9 **(b)**. Single thick, dashed horizontal line denotes 1 – PIP threshold (see main text). The thin dashed lines specific to each bar denotes (1 – average PIP) (where average is taken across all genetic elements belonging to that bar; see main text). **(c,d)** Average gene fine-mapping power across 100 simulations for various fine-mapping methods (see legend) across eQTL sample sizes (x-axis) at PIP=0.5 **(c)** and PIP=0.9 **(d)**. Error bars denote 95% confidence intervals. This supplementary figure resembles figure 1, except it shows calibration and power of gene fine-mapping, instead of tissue-gene fine-mapping. “TGFM” corresponds to TGFM (Gene). “FOCUS-TG” corresponds to running FOCUS applied to the task of tissue-gene fine-mapping, and then summing PIPs across tissues. “FOCUS” corresponds to running FOCUS in each tissue, independently, and taking the maximum FOCUS PIP across tissues for each gene. “coloc” corresponds to running coloc in each tissue, independently, and taking the maximum coloc PPH4 across tissues for each gene.

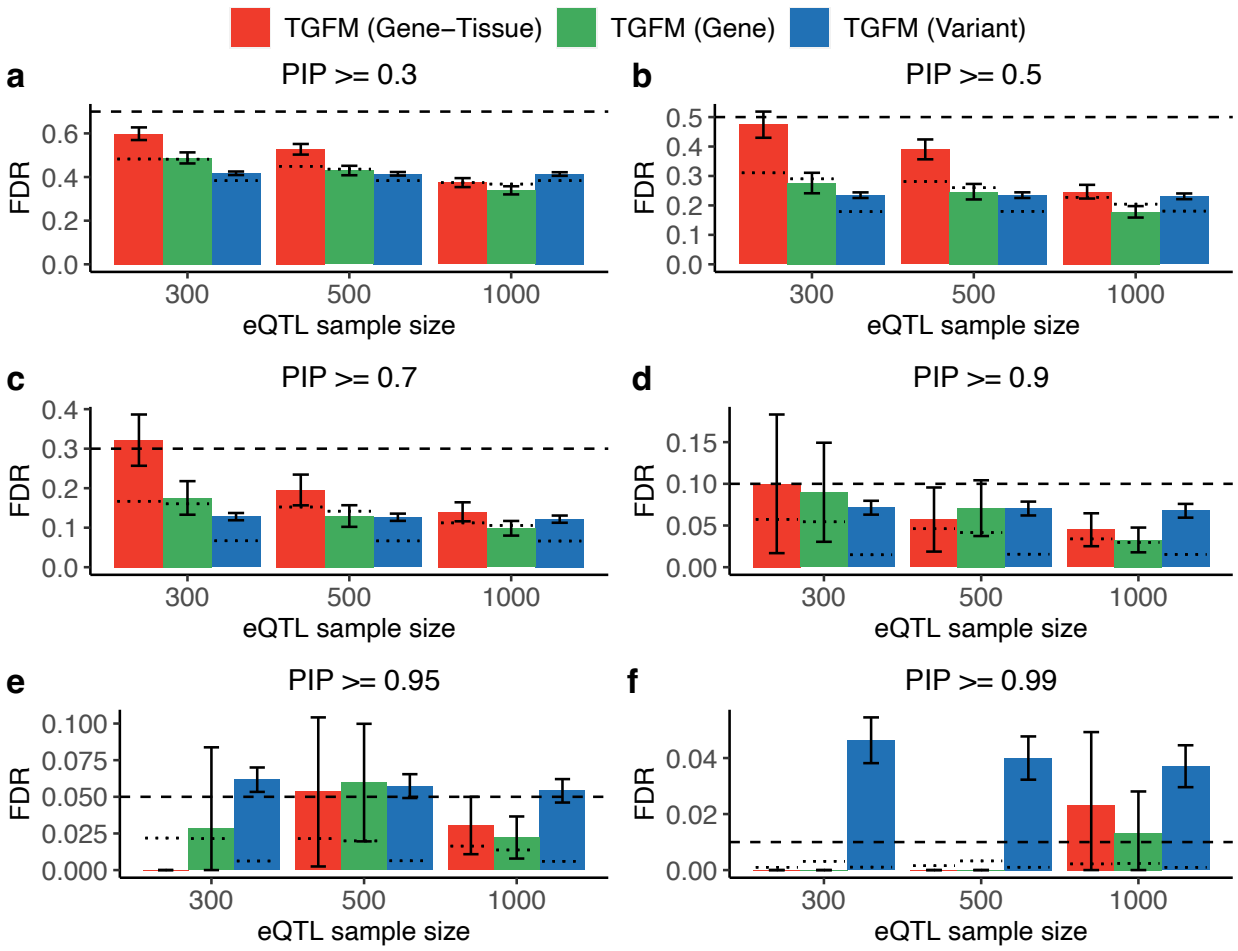

Supplementary Figure 4: Calibration of fine-mapping genetic elements with TGFM at various PIP thresholds in simulations. (a,b) Average fine-mapping FDR across 100 simulations using TGFM for different classes of genetic elements (see legend) across eQTL sample sizes (x-axis) at PIP=0.3 **(a)**, PIP=0.5 **(b)**, PIP=0.7 **(c)**, PIP=0.9 **(d)**, PIP=0.95 **(e)**, and PIP=0.99 **(f)**. In each plot, the single thick-dashed horizontal line (1 – PIP) threshold (see main text). The thin dashed lines specific to each bar denotes (1 – average PIP) (where average is taken across all genetic elements belonging to that bar; see main text). Error bars denote 95% confidence intervals. This supplementary figure is the same as Fig. 2a-b, except it includes more PIP thresholds, as well as dashed lines denoting (1 – average PIP).

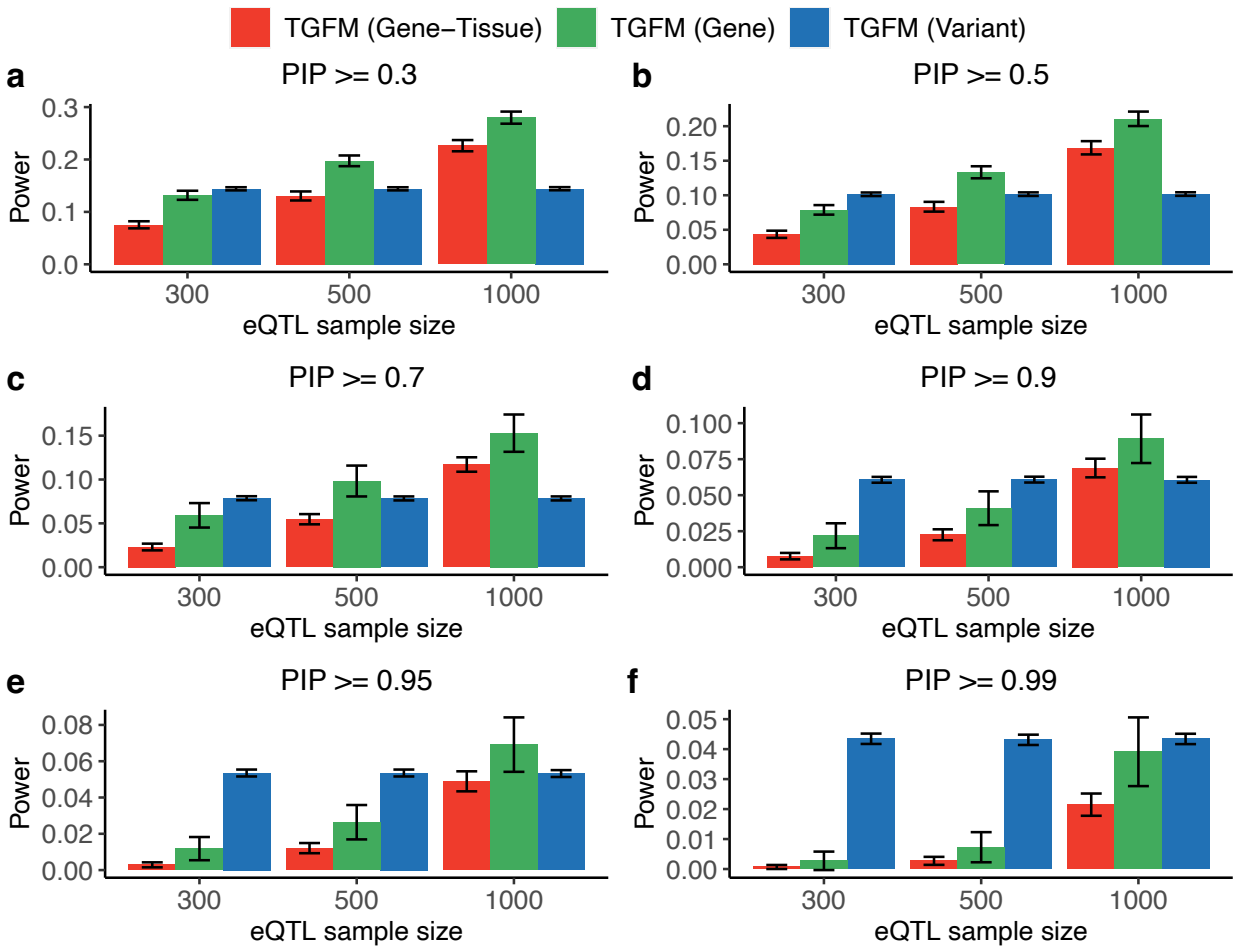

Supplementary Figure 5: Power of fine-mapping genetic elements with TGFM at various PIP thresholds in simulations. Average fine-mapping power across 100 simulations using TGFM for different classes of genetic elements (see legend) across eQTL sample sizes (x-axis) at PIP=0.3 **(a)**, PIP=0.5 **(b)**, PIP=0.7 **(c)**, PIP=0.9 **(d)**, PIP=0.95 **(e)**, and PIP=0.99 **(f)**. Error bars denote 95% confidence intervals. This supplementary figure is the same as Fig. 1c-d, except it includes more PIP thresholds.

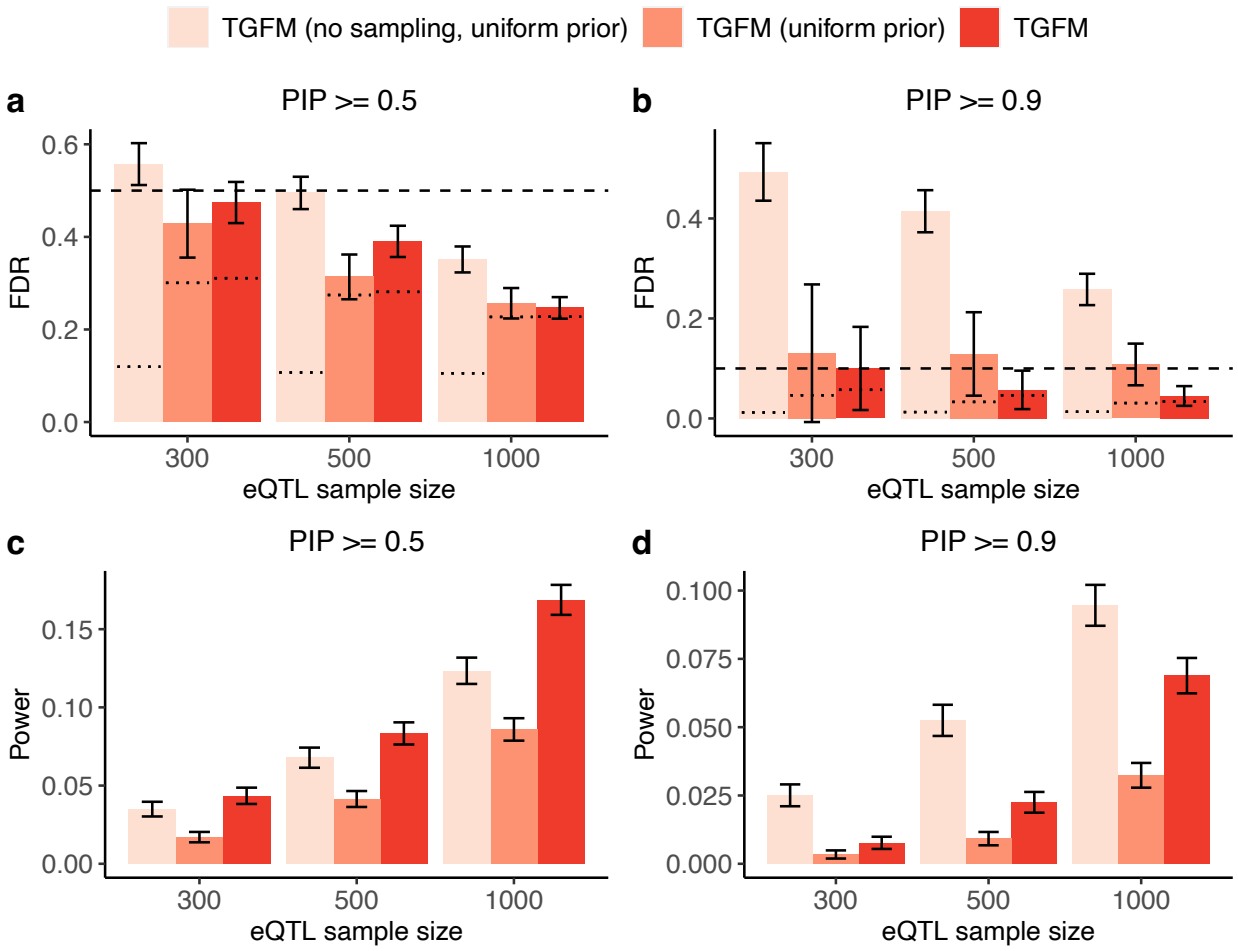

Supplementary Figure 6: Calibration and power of tissue-gene fine-mapping for various versions of TGFM in simulations. (a,b) Average tissue-gene fine-mapping FDR across 100 simulations for various fine-mapping methods (see legend) across eQTL sample sizes (x-axis) at PIP=0.5 **(a)** and PIP=0.9 **(b)**. Single thick, dashed horizontal line denotes 1 – PIP threshold (see main text). The thin dashed horizontal lines specific to each bar denotes (1 – average PIP) (where average is taken across all genetic elements belonging to that bar; see main text). **(c,d)** Average tissue-gene fine-mapping power across 100 simulations for various fine-mapping methods (see legend) across eQTL sample sizes (x-axis) at PIP=0.5 **(c)** and PIP=0.9 **(d)**. Error bars denote 95% confidence intervals. This supplementary figure resembles figure 1, except it shows calibration and power of additional tissue-gene fine-mapping methods. “TGFM (no sampling, uniform prior)” corresponds to TGFM (Gene-Tissue) with a uniform prior and a single cis-predicted expression model (based on posterior mean causal cis-eQTL effect sizes) instead of averaging results across 100 sampled cis-predicted expression models. “TGFM (uniform prior)” corresponds to TGFM (Gene-Tissue) with a uniform prior. “TGFM” corresponds to the default version of TGFM (Gene-Tissue) (shown in Figure 1).

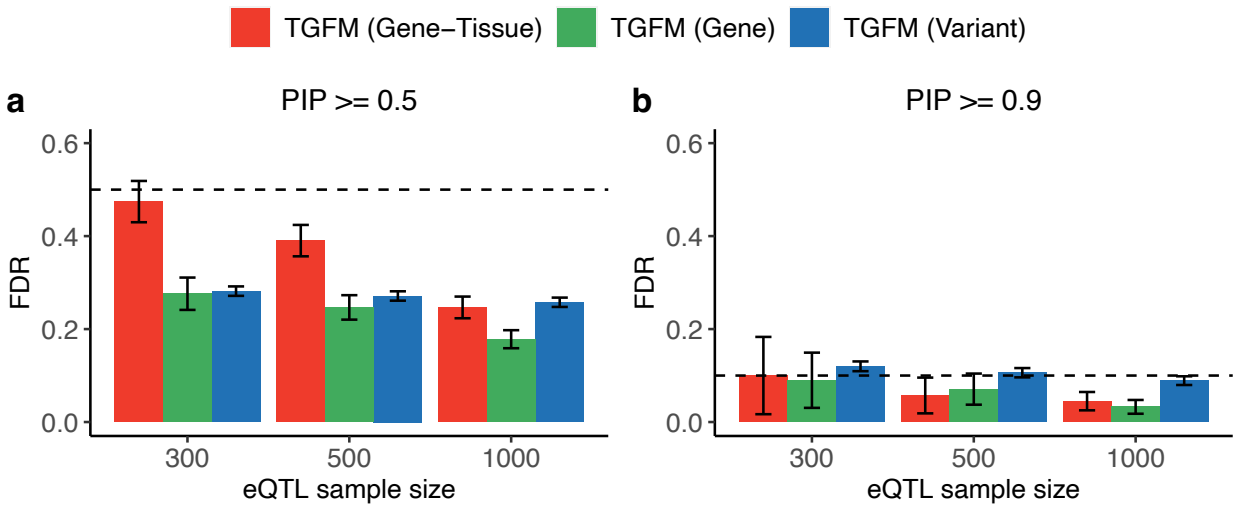

Supplementary Figure 7: Calibration of fine-mapping genetic elements with TGFM at various PIP thresholds in simulations using alternative definition of false-positive variants. Average fine-mapping FDR across 100 simulations using TGFM for different classes of genetic elements (see legend) across eQTL sample sizes (x-axis) at PIP=0.5 **(a)** and PIP=0.9. Dashed horizontal line denotes 1 – PIP threshold (see main text). Error bars denote 95% confidence intervals. Unlike Figure 2a-b, causal eQTL variants for causal gene-tissue pairs were considered false positives for variant-level calibration. TGFM (Variant) is mis-calibrated at eQTL sample size=300 and PIP >= 0.9. The calibration worsened at small eQTL sample sizes, likely due to decreased power to detect causal gene-tissue pairs at small eQTL sample sizes, forcing the unmodeled gene-tissue pair effects to be captured by non-mediated variants.

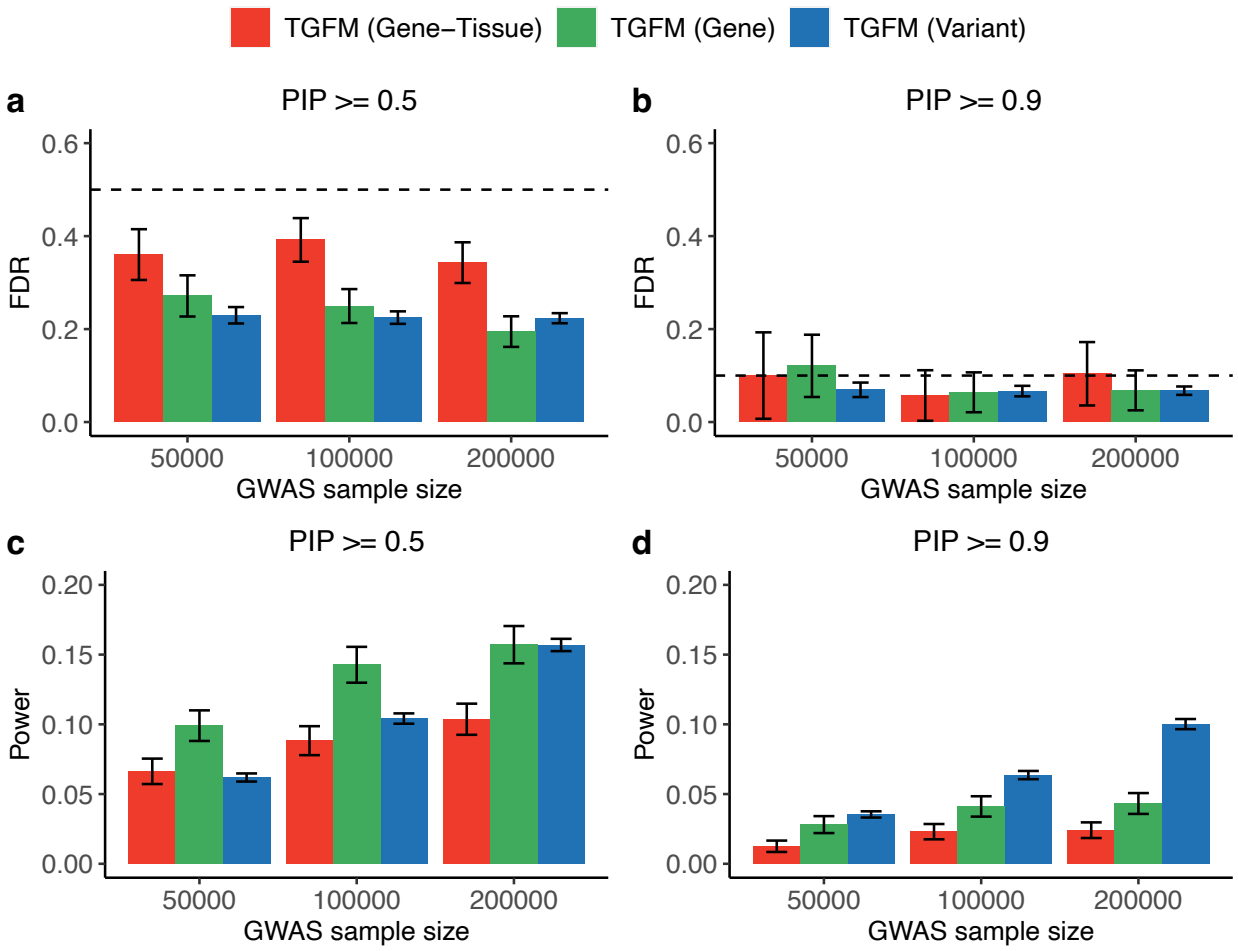

Supplementary Figure 8: Calibration and power of fine-mapping different classes of genetic elements with TGFM in simulations for various simulated GWAS sample sizes. (a,b) Average fine-mapping FDR across 50 simulations using TGFM for different classes of genetic elements (see legend) across GWAS sample sizes (x-axis) at PIP=0.5 **(a)** and PIP=0.9 **(b)** at eQTL sample size of 500. Dashed horizontal line denotes 1 – PIP threshold (see main text). **(c,d)** Average fine-mapping power across 50 simulations using TGFM for different classes of genetic elements (see legend) across GWAS sample sizes (x-axis) at PIP=0.5 **(c)** and PIP=0.9 **(d)** at eQTL sample size of 500. Error bars denote 95% confidence intervals. This supplementary figure is the same as Figure 2, except it shows results at a fixed eQTL sample of 500, and varies the GWAS sample size.

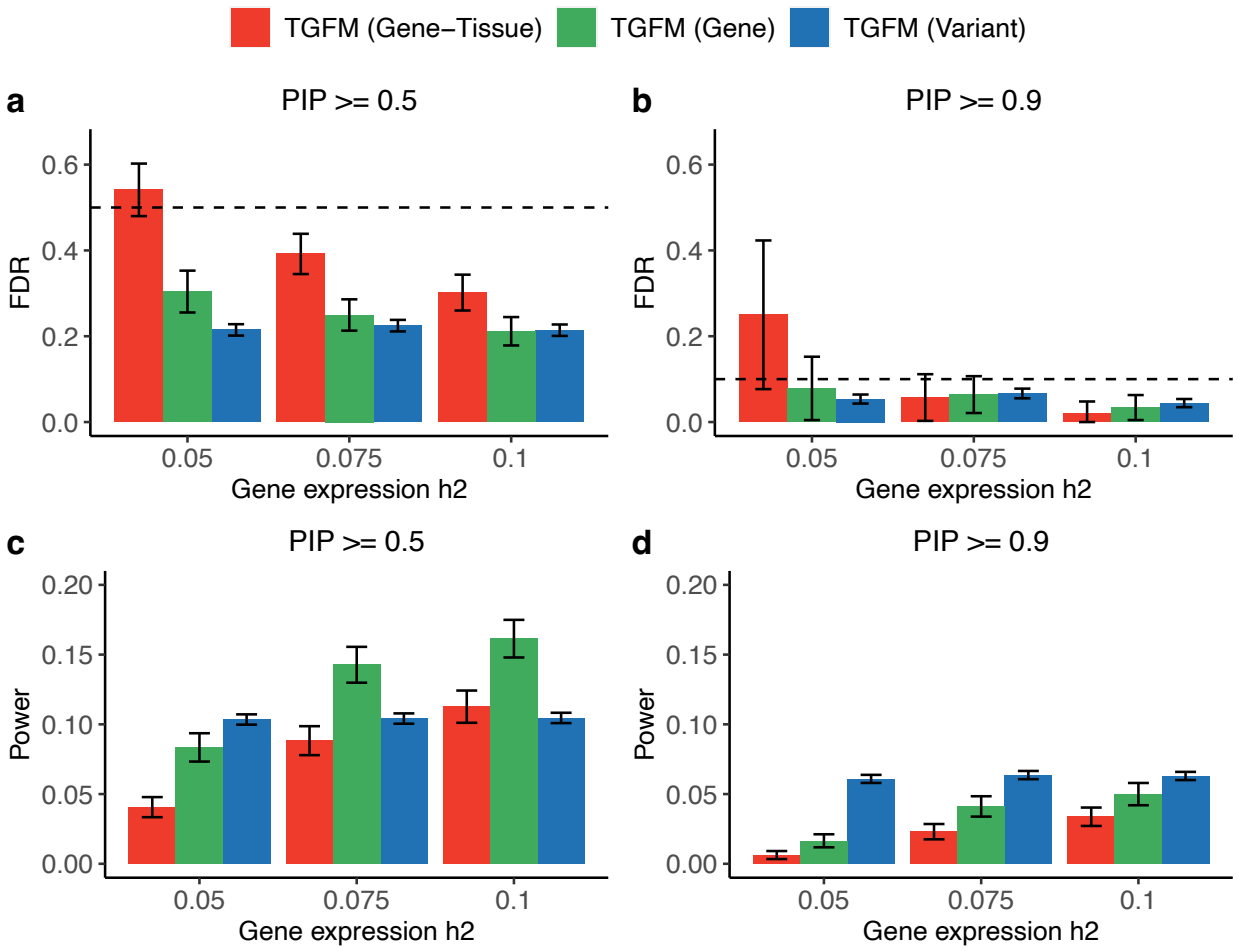

Supplementary Figure 9: Calibration and power of fine-mapping different classes of genetic elements with TGFM in simulations for various simulated gene expression heritabilities. (a,b) Average fine-mapping FDR across 50 simulations using TGFM for different classes of genetic elements (see legend) across simulated gene expression heritabilities (x-axis) at PIP=0.5 **(a)** and PIP=0.9 **(b)** at eQTL sample size of 500. Dashed horizontal line denotes 1 – PIP threshold (see main text). **(c,d)** Average fine-mapping power across 50 simulations using TGFM for different classes of genetic elements (see legend) across simulated gene expression heritabilities (x-axis) at PIP=0.5 **(c)** and PIP=0.9 **(d)** at eQTL sample size of 500. Error bars denote 95% confidence intervals. This supplementary figure is the same as Figure 2, except it shows results at a fixed eQTL sample of 500, and varies the gene expression heritability.

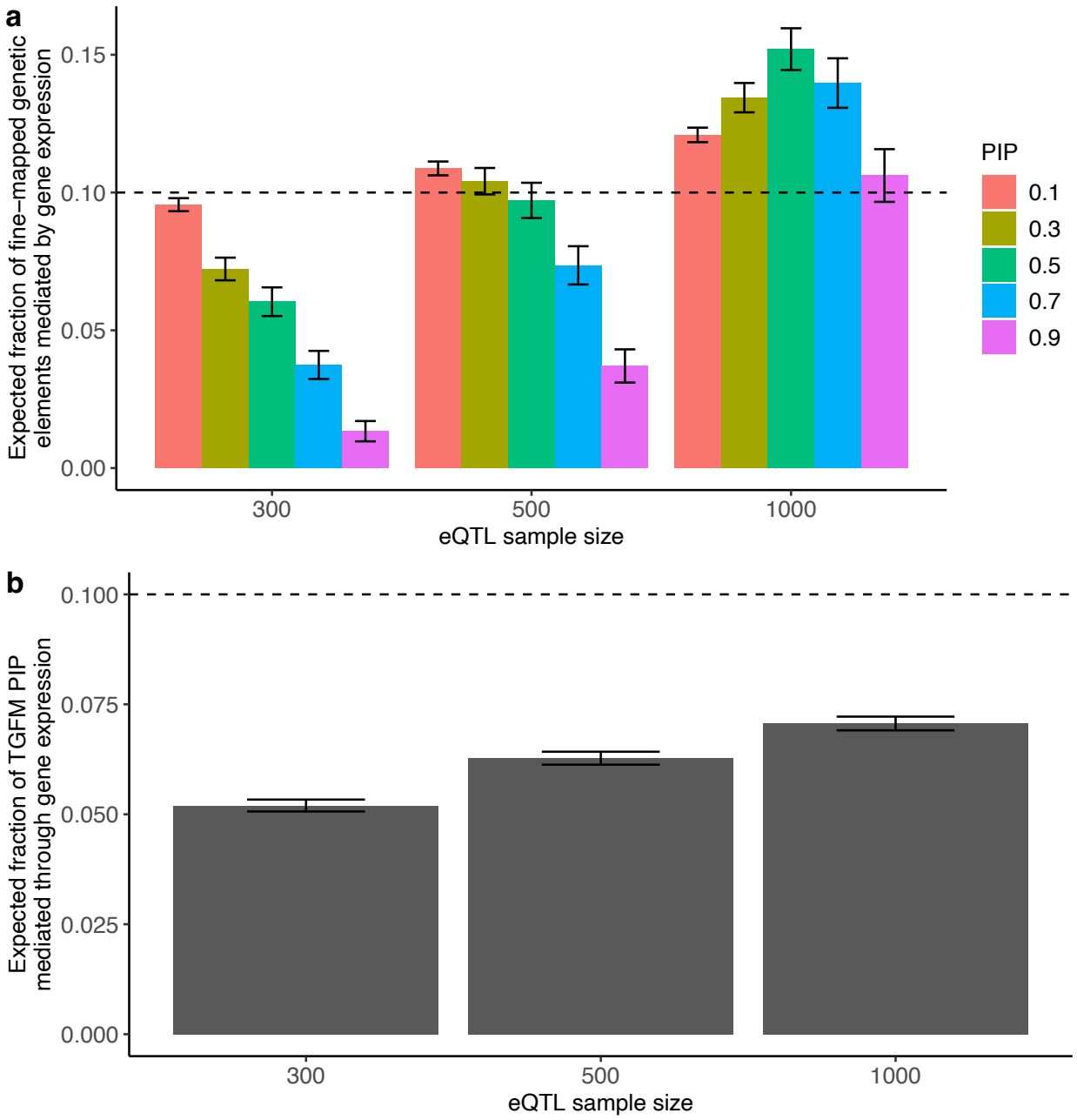

Supplementary Figure 10: Evaluating bias in estimating the proportion of genetic elements that are gene-tissue pairs in simulations. The horizontal dashed line in plot **(a)** and **(b)** represents the simulated, true proportion of genetic elements that are gene-tissue pairs. **(a)** We report the average proportion of fine-mapped genetic elements across 100 simulations that are gene-tissue pairs (y-axis) at various PIP thresholds (see legend) across various eQTL sample sizes (x-axis). This approach yielded either upward or downward biased estimates of the true proportion depending on eQTL sample size and PIP threshold, reflecting differential discovery power of non-mediated variants and gene-tissue pairs as a function of both eQTL sample size and PIP threshold. **(b)** We report the average expected proportion of causal genetic elements

that are gene-tissue pairs (y-axis) across 100 simulations (computed by summing PIPs across genetic elements), shown at various eQTL sample sizes (x-axis). This approach yielded conservative estimates of the true proportion, becoming less conservative at larger eQTL sample sizes, suggesting that this statistic can provide a conservative lower bound on the true proportion of causal genetic elements that are gene-tissue pairs. Error bars denote 95% confidence intervals.

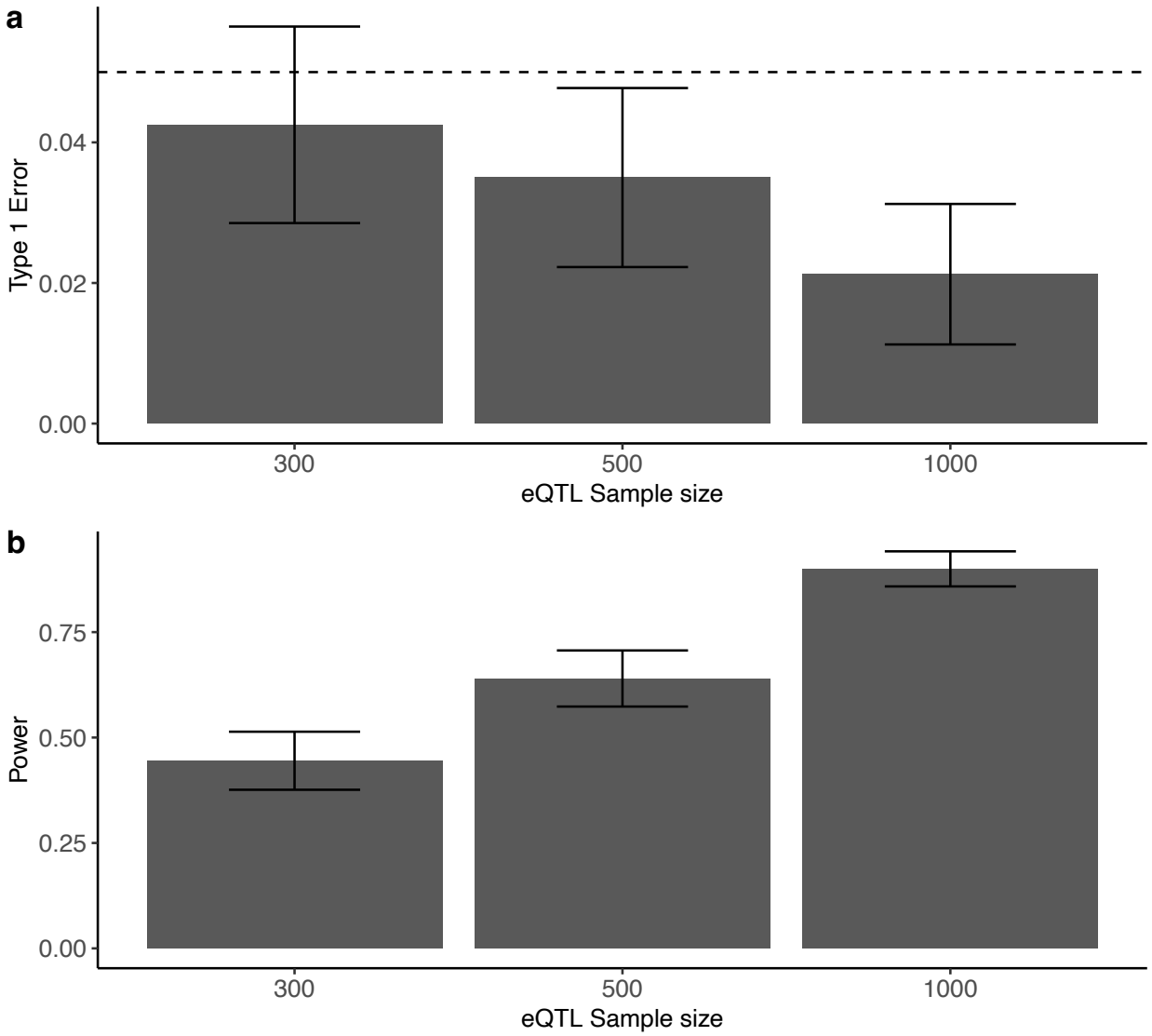

Supplementary Figure 11: Evaluating power and type 1 error of identifying disease-critical tissues using the TGFM tissue-specific prior in simulations. (a) Average type 1 error across 100 simulations for identifying disease-critical tissues using the TGFM tissue-specific prior at a p-value threshold of 0.05 (y-axis) at various eQTL sample sizes (x-axis). Error bars denote 95% confidence intervals. **(b)** Average power across 100 simulations for identifying disease-critical tissues using the TGFM tissue-specific prior at a p-value threshold of 0.05 (y-axis) at various eQTL sample sizes (x-axis). Error bars represent 95% confidence intervals.

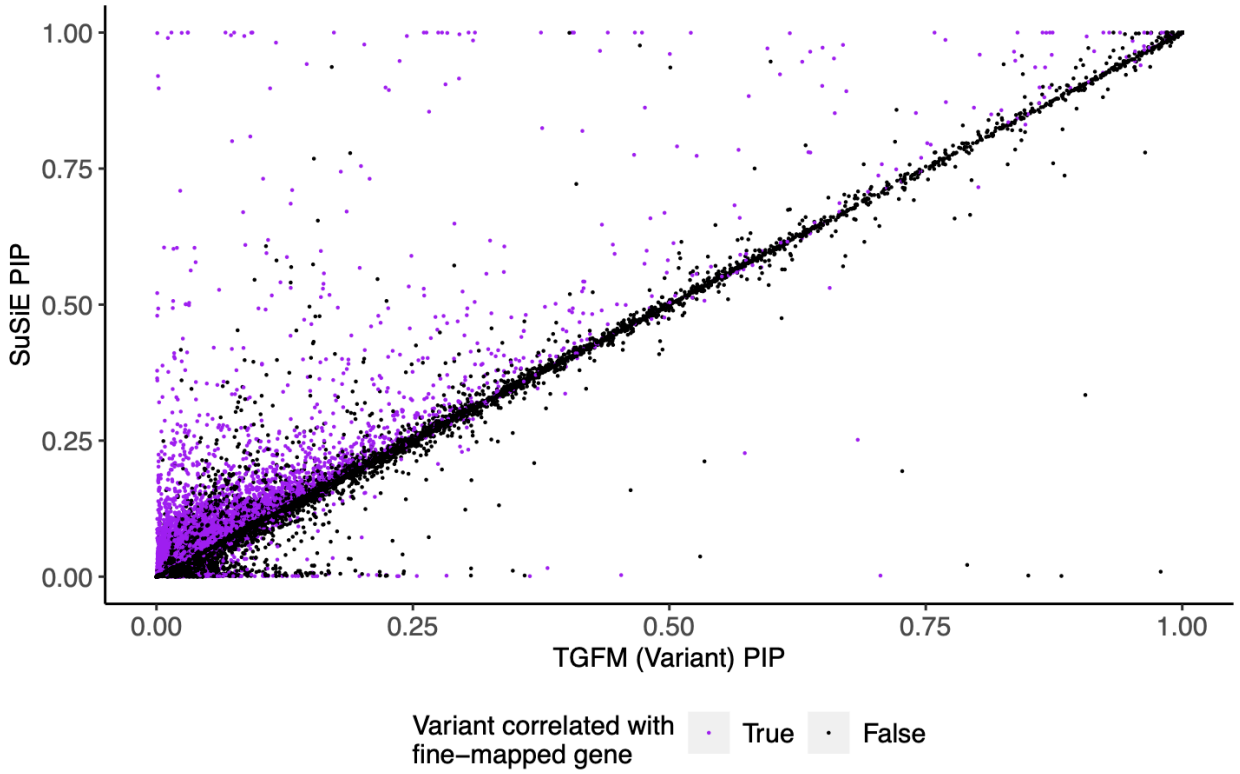

Supplementary Figure 12: Direct comparison of TGFM (Variant) PIPs and SuSiE PIPS in simulations. For each non-mediated variant analyzed across 20 default simulations at eQTL sample size of 500, we plot the TGFM (Variant) PIP (x-axis) and the SuSiE PIP (y-axis) colored by whether the variant had absolute correlation > 0.25 with a fine-mapped (PIP > 0.05) gene-tissue pair. The correlation across all variants was 0.975 (slope of regression of SuSiE PIP on TGFM (Variant) PIP: 1.016), the correlation across all variants not correlated with a fine-mapped gene-tissue pair (black points) was 0.993 (slope: 0.999), and the correlation across all variants correlated with a fine-mapped gene-tissue pair (purple points) was 0.889 (slope: 1.160). For strictly visualization purposes, we only visualize a random subset of 100,000 variants with both SuSiE PIP < 0.01 and TGFM (Variant) PIP < 0.01.

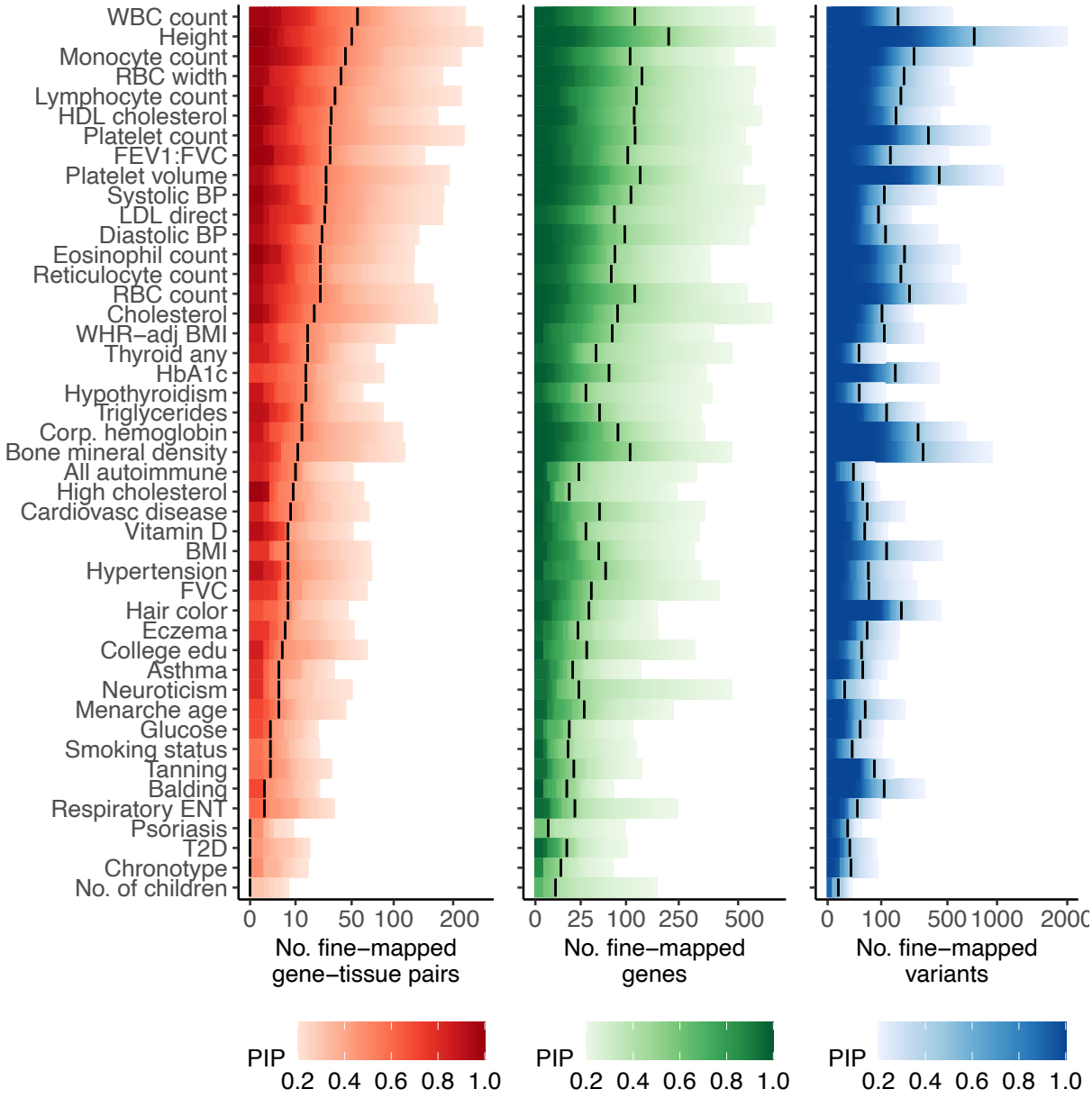

Supplementary Figure 13: Summary of fine-mapping genetic elements with TGFM for all 45 UK Biobank disease and traits. We report the number of **(a)** Gene-tissue pairs, **(b)** Genes, and **(c)** (non-mediated) Variants fine-mapped using TGFM (x-axis; square root scale) across 45 UK Biobank traits (y-axis) at various PIP thresholds ranging from 0.2 to 1.0 (color-bars). Vertical black lines denote the number of genetic elements fine-mapped at PIP=0.5. This supplementary figure is the same as Figure 3, except it shows results across all 45 traits, and the x-axis and y-axis are flipped.

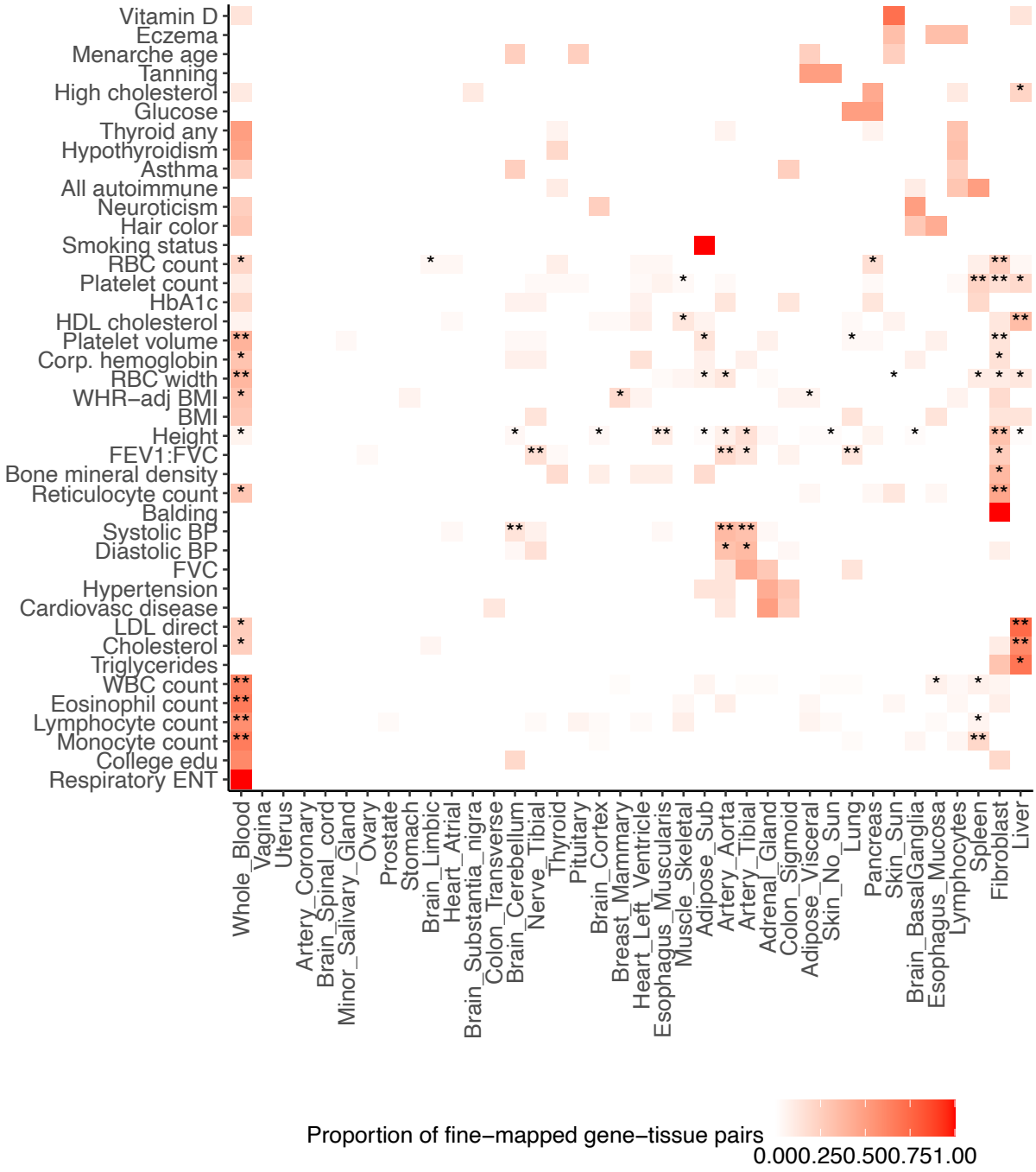

Supplementary Figure 14: Proportion of fine-mapped gene-tissue pairs in each tissue for all traits. Proportion of fine-mapped gene-tissue pairs in each tissue (x-axis) for 45 traits (y-axis). Proportions for each trait were calculated by counting the number of gene-tissue pairs with TGFM PIP > 0.5 in each tissue and normalizing the counts across tissues. Statistical significance of each tissue-disease pair by applying genomic bootstrapping to the TGFM tissue-specific prior. ** represents FDR ≤ 0.05, and $*$ represents FDR ≤ 0.2. Numerical results are reported in Supplementary Table 9.

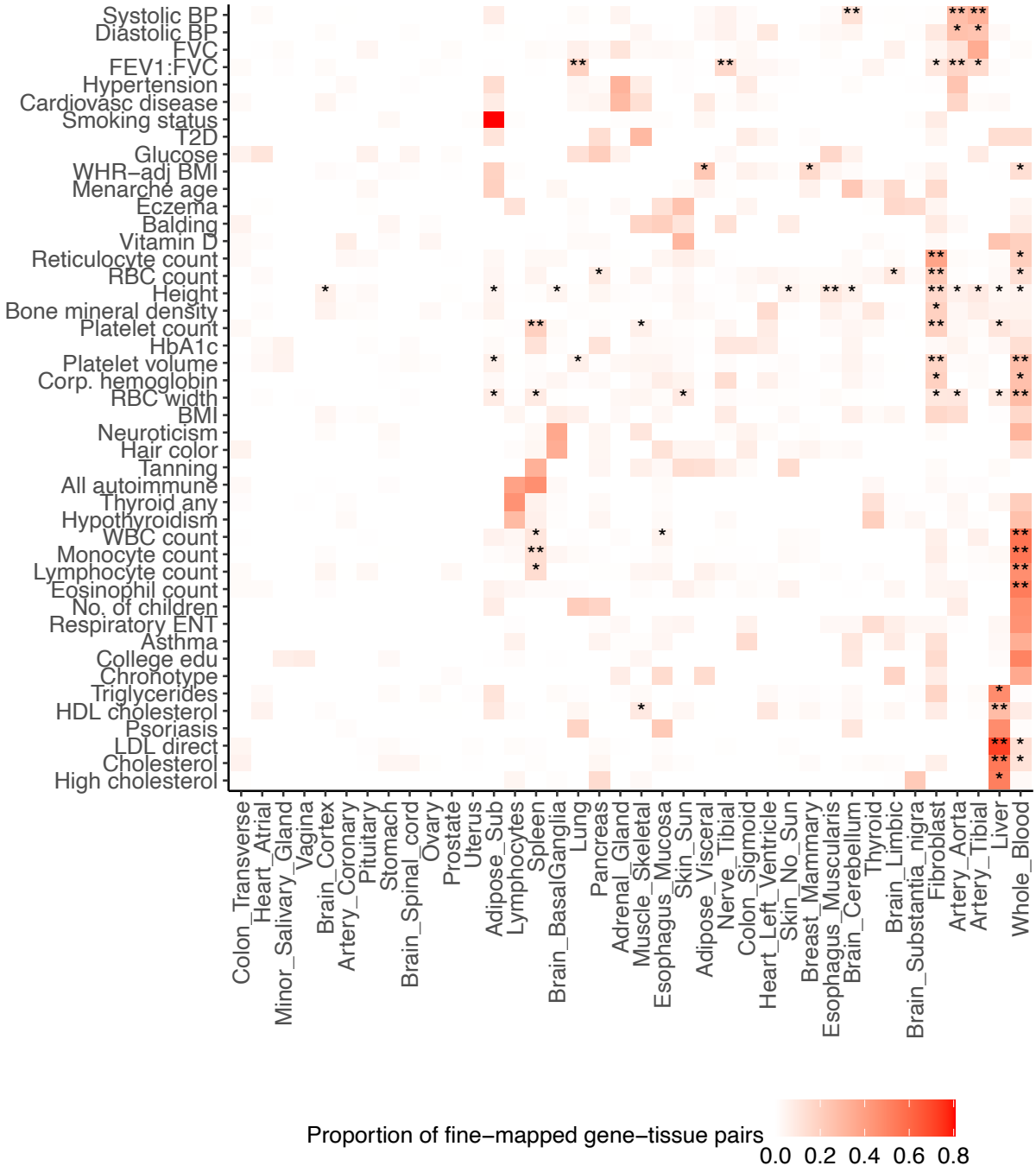

Supplementary Figure 15: Proportion of fine-mapped gene-tissue pairs in each tissue for all traits at alternative threshold (PIP $>$ 0.1). Proportion of fine-mapped gene-tissue pairs in each tissue (x-axis) for 45 traits (y-axis). Proportions for each trait were calculated by counting the number of gene-tissue pairs with TGFM PIP > 0.1 in each tissue and normalizing the counts across tissues. Statistical significance of each tissue-disease pair by applying genomic bootstrapping to the TGFM tissue-specific prior. ** represents FDR ≤ 0.05, and $*$ represents FDR ≤ 0.2.

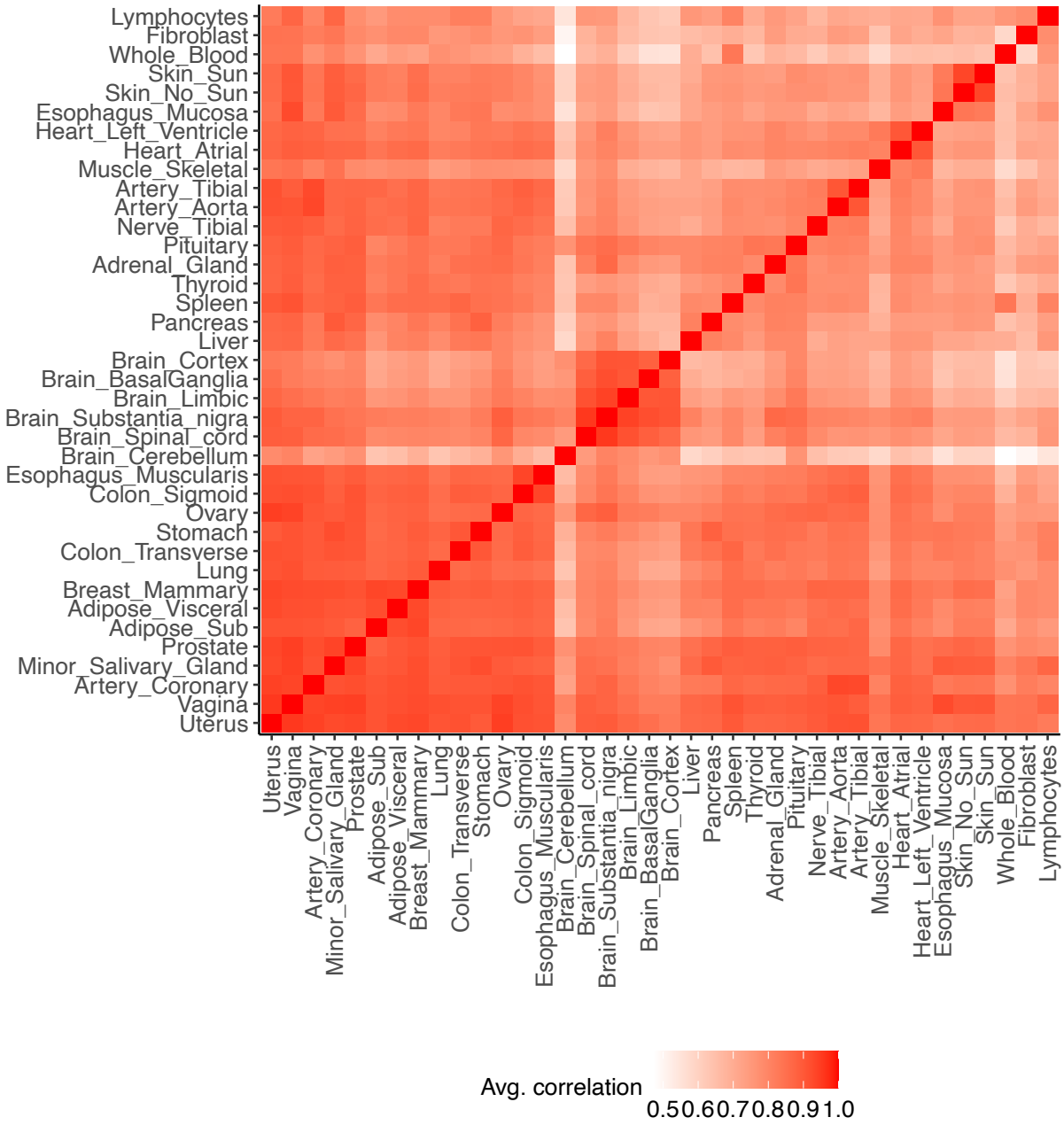

Supplementary Figure 16: Average correlation in cis-predicted gene expression between pairs of GTEx tissues. We report the average correlation in cis-predicted gene expression between each pair of GTEx tissues across all genes included in TGFM. For a given pair of tissues, we only compute the correlation across genes with a cis-predicted expression model in both tissues. We observed that several of the low sample size tissues (e.g. uterus, vagina, artery coronary, minor salivary gland, prostate; Supplementary Table 6) have high correlation with nearly all other tissues. We assume this is a technical artifact of low sample size tissues being limited to discovering very large eQTL effect size variants (due to statistical power), which are known to be less tissue-specific than small eQTL effect size variants.

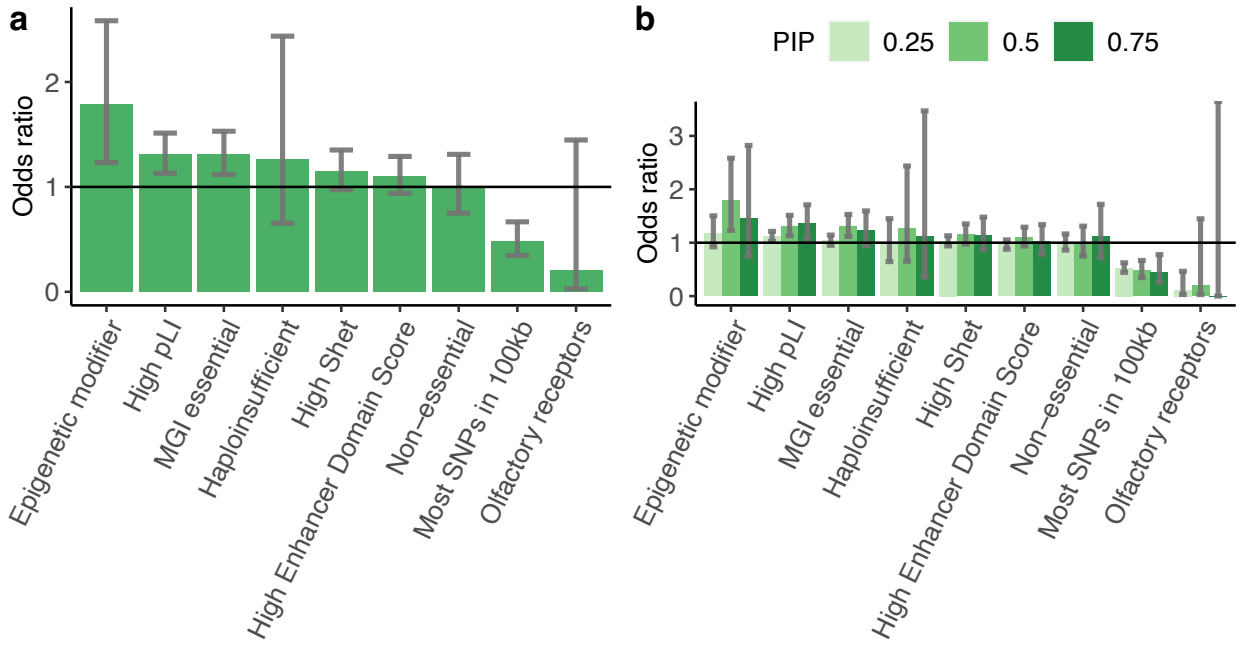

Supplementary Figure 17: Enrichment of fine-mapped TGFM genes within non-disease-specific gene sets. (a) Enrichment of genes with TGFM (Gene) PIP > 0.5 within non-disease-specific gene sets meta-analyzed over 16 independent traits. Error bars represent 95% confidence intervals. Odds ratios and standard errors on the odds ratio were computed using logistic regression. **(b)** Enrichment of genes with TGFM (Gene) PIP > 0.25, 0.5, and 0.75 (see legend) within non-disease-specific gene sets meta-analyzed over 16 independent traits. Error bars represent 95% confidence intervals. Odds ratios and standard errors on the odds ratio were computed using logistic regression. Numerical results reported in Supplementary Table 12.

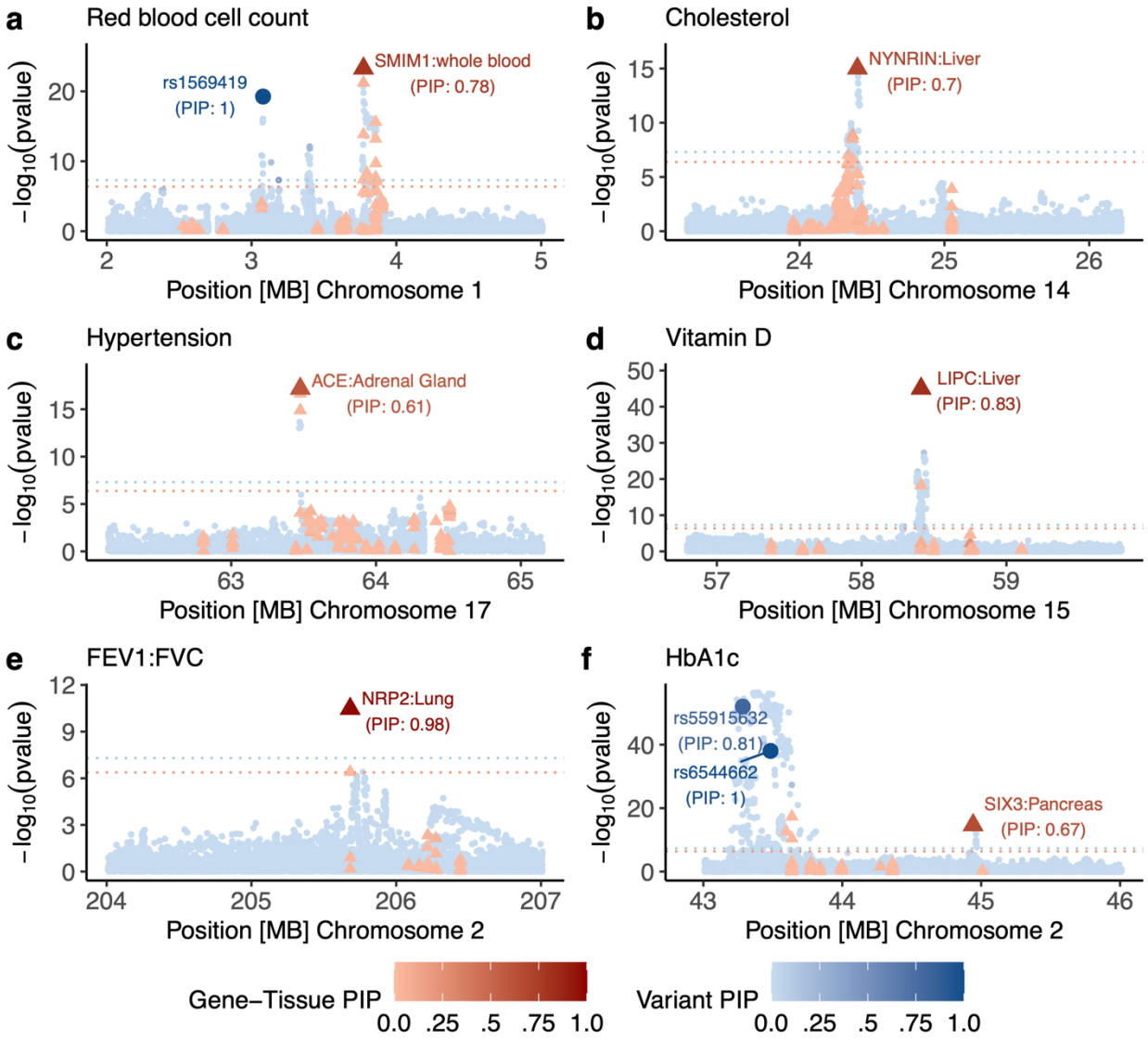

Supplementary Figure 18: Additional examples of fine-mapped gene-tissue-disease triplets identified by TGFM. We report 6 example loci for which TGFM fine-mapped a gene-tissue pair (PIP > 0.5). In each example we report the marginal GWAS and TWAS association -$\log_{10}$ p-values (y-axis) of non-mediated variants (blue circles) and gene-tissue pairs (red triangles). Marginal TWAS association -$\log_{10}$ p-values were calculated by taking the median -$\log_{10}$ TWAS p-value across the 100 sets of sampled cis-predicted expression models for each gene-tissue pair. The genomic position of each gene-tissue pair (x-axis) was based on the gene's TSS. The color shading of each variant and gene-tissue pair was determined by its TGFM PIP. Any genetic element with TGFM PIP > 0.5 was made larger in size. Dashed horizontal blue and red lines represent GWAS significance (5×10^{-8}) and TWAS significance (4.2×10^{-7}) thresholds, respectively.

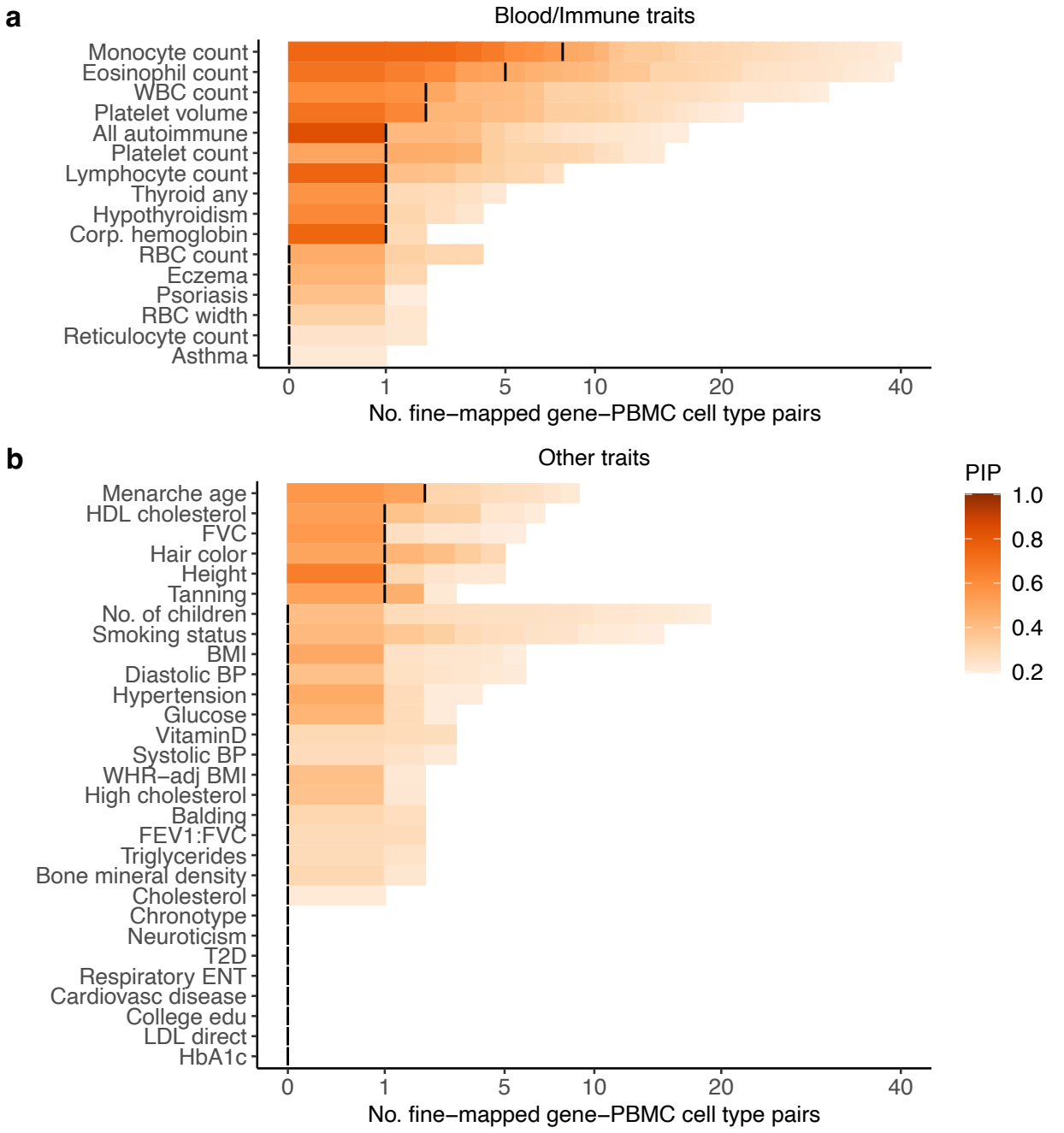

Supplementary Figure 19*: Summary of fine-mapping gene-PBMC cell type pairs with TGFM for all 45 UK Biobank diseases and traits.* Number of gene-PBMC cell type pairs fine-mapped using TGFM (x-axis; square root scale) across 18 representative UK Biobank traits (y-axis) at various PIP thresholds ranging from 0.2 to 1.0 (color-bar), distinguishing between **(a)** autoimmune diseases and blood cell traits and **(b)** non-blood-related traits. Vertical black lines denote the number of gene-PBMC cell type pairs fine-mapped at PIP=0.5. Numerical results are reported in Supplementary Table 15. This supplementary figure is the same as Figure 6a-b, except it shows results across all 45 traits, and the x-axis and y-axis are flipped.

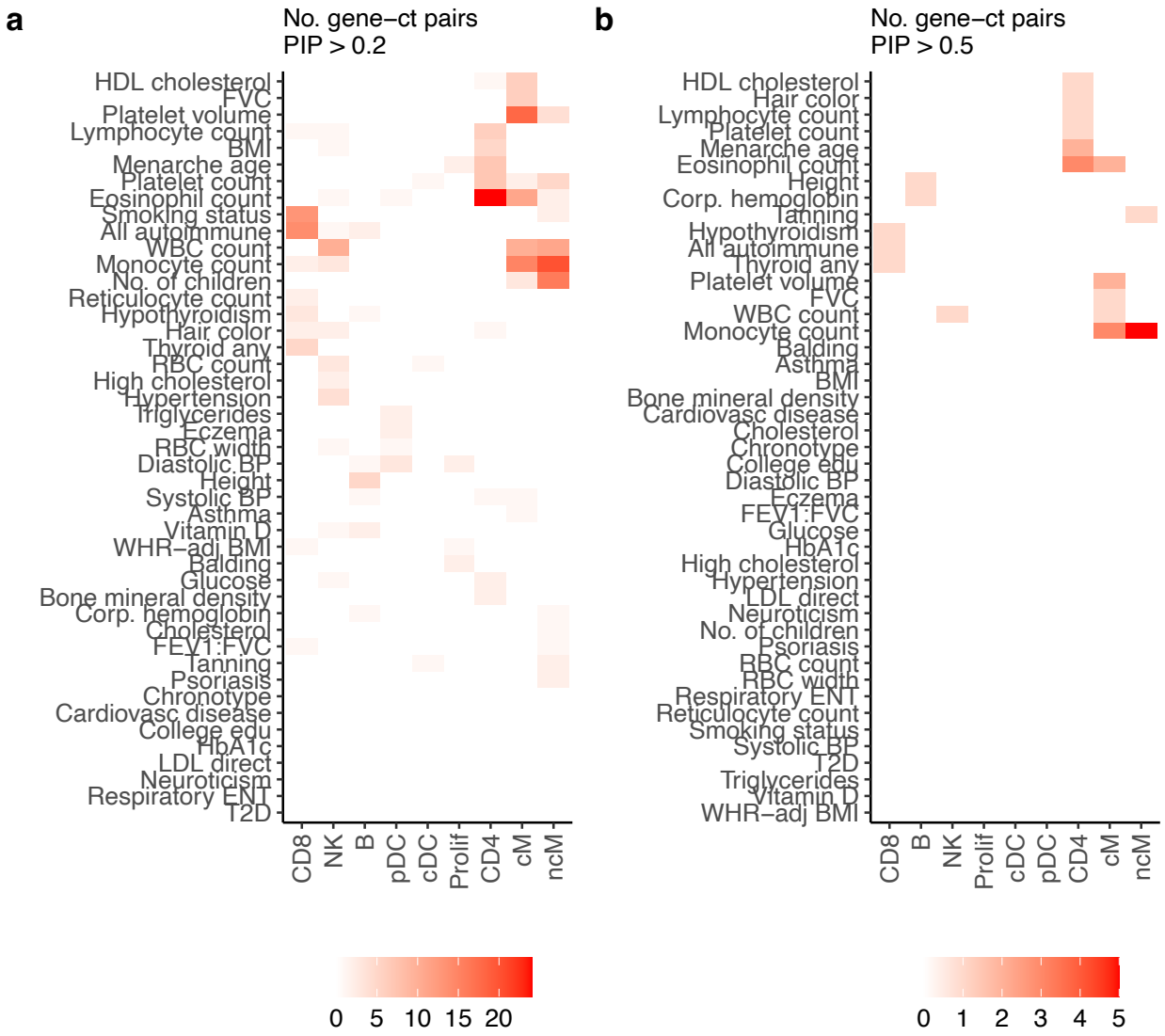

Supplementary Figure 20*: Number of gene-PBMC cell type pairs corresponding to each trait-PBMC cell type across 45 UK Biobank diseases and traits.* The number of fine-mapped gene-PBMC cell type pairs at PIP > 0.2 **(a)** and PIP > 0.5 **(b)** corresponding to each trait-PBMC cell type pair across 45 UK Biobank diseases and traits. Numerical results are reported in Supplementary Table 15.

References

1. Cvejic, A. *et al.* SMIM1 underlies the Vel blood group and influences red blood cell traits. *Nat. Genet.* **45**, 542–545 (2013).
2. Aniweh, Y., Nyarko, P. B., Quansah, E., Thiam, L. G. & Awandare, G. A. SMIM1 at a glance; discovery, genetic basis, recent progress and perspectives. *Parasite Epidemiol. Control* **5**, e00101 (2019).
3. Weeks, E. M. *et al.* Leveraging polygenic enrichments of gene features to predict genes underlying complex traits and diseases. *Nat. Genet.* **55**, 1267–1276 (2023).
4. van der Harst, P. *et al.* Seventy-five genetic loci influencing the human red blood cell. *Nature* **492**, 369–375 (2012).
5. Talmud, P. J. *et al.* Use of low-density lipoprotein cholesterol gene score to distinguish patients with polygenic and monogenic familial hypercholesterolaemia: a case-control study. *Lancet* **381**, 1293–1301 (2013).
6. Olmastroni, E. *et al.* Twelve variants polygenic score for low-density lipoprotein cholesterol distribution in a large cohort of patients with clinically diagnosed familial hypercholesterolemia with or without causative mutations. *J. Am. Heart Assoc.* **11**, (2022).
7. Schlueter, W., Keilani, T. & Batlle, D. C. Tissue renin angiotensin systems: theoretical implications for the development of hyperkalemia using angiotensin-converting enzyme inhibitors. *Am. J. Med. Sci.* **307 Suppl 1**, S81-6 (1994).
8. Coates, D. The angiotensin converting enzyme (ACE). *Int. J. Biochem. Cell Biol.* **35**, 769–773 (2003).

9. Sayed-Tabatabaei, F. A., Oostra, B. A., Isaacs, A., van Duijn, C. M. & Witteman, J. C. M. *ACE* polymorphisms. *Circ. Res.* **98**, 1123–1133 (2006).
10. Wang, Y. & Wang, J.-G. Genome-wide association studies of hypertension and several other cardiovascular diseases. *Pulse (Basel)* **6**, 169–186 (2018).
11. Connelly, P. W. The role of hepatic lipase in lipoprotein metabolism. *Clin. Chim. Acta* **286**, 243–255 (1999).
12. Santamarina-Fojo, S., Haudenschild, C. & Amar, M. The role of hepatic lipase in lipoprotein metabolism and atherosclerosis. *Curr. Opin. Lipidol.* **9**, 211–219 (1998).
13. Manousaki, D. *et al.* Genome-wide association study for vitamin D levels reveals 69 independent loci. *Am. J. Hum. Genet.* **106**, 327–337 (2020).
14. Li, Y. *et al.* Association of changes in lipid levels with changes in vitamin D levels in a real-world setting. *Sci. Rep.* **11**, 1–7 (2021).
15. Hyppönen, E., Vimaleswaran, K. S. & Zhou, A. Genetic determinants of 25-hydroxyvitamin D concentrations and their relevance to public health. *Nutrients* **14**, 4408 (2022).
16. Mancuso, N. *et al.* Probabilistic fine-mapping of transcriptome-wide association studies. *Nat. Genet.* **51**, 675–682 (2019).
17. Ongen, H. *et al.* Estimating the causal tissues for complex traits and diseases. *Nat. Genet.* **49**, 1676–1683 (2017).
18. Finucane, H. K. *et al.* Heritability enrichment of specifically expressed genes identifies disease-relevant tissues and cell types. *Nat. Genet.* **50**, 621–629 (2018).
19. Amariuta, T., Siewert-Rocks, K. & Price, A. L. Modeling tissue co-regulation estimates tissue-specific contributions to disease. *Nat. Genet.* **55**, 1503–1511 (2023).

20. Immormino, R. M., Jania, C. M., Tilley, S. L. & Moran, T. P. Neuropilin-2 regulates airway inflammation in a neutrophilic asthma model. *Immun. Inflamm. Dis.* **10**, (2022).
21. Wang, B. *et al.* Alveolar macrophage-derived NRP2 curtails lung injury while boosting host defense in bacterial pneumonia. *J. Leukoc. Biol.* **112**, 499–512 (2022).
22. Arda, H. E. *et al.* Age-dependent pancreatic gene regulation reveals mechanisms governing human β cell function. *Cell Metab.* **23**, 909–920 (2016).
23. Bevacqua, R. J. *et al.* SIX2 and SIX3 coordinately regulate functional maturity and fate of human pancreatic β cells. *Genes Dev.* **35**, 234–249 (2021).